



# Investigation of the parallel gradation method based on the response of track-bed materials under cyclic loadings

Shuai Qi, Yu Jun Cui, Jean Claude Dupla, Ren-Peng Chen, Han-Lin Wang,  
Yu Su, Francisco Lamas-Lopez, Jean Canou

## ► To cite this version:

Shuai Qi, Yu Jun Cui, Jean Claude Dupla, Ren-Peng Chen, Han-Lin Wang, et al.. Investigation of the parallel gradation method based on the response of track-bed materials under cyclic loadings. Transportation Geotechnics, 2020, 24, pp.100360. 10.1016/j.trgeo.2020.100360 . hal-03045872

**HAL Id: hal-03045872**

**<https://enpc.hal.science/hal-03045872>**

Submitted on 28 May 2021

**HAL** is a multi-disciplinary open access archive for the deposit and dissemination of scientific research documents, whether they are published or not. The documents may come from teaching and research institutions in France or abroad, or from public or private research centers.

L'archive ouverte pluridisciplinaire **HAL**, est destinée au dépôt et à la diffusion de documents scientifiques de niveau recherche, publiés ou non, émanant des établissements d'enseignement et de recherche français ou étrangers, des laboratoires publics ou privés.

**Investigation of the parallel gradation method based on the response of  
track-bed materials under cyclic loadings**

Shuai Qi<sup>1, 2</sup>, Yu-Jun Cui<sup>2</sup>, Jean-Claude Dupla<sup>2</sup>, Ren-Peng Chen<sup>1</sup>, Han-Lin Wang<sup>3</sup>, Yu  
Su<sup>2</sup>, Francisco Lamas-Lopez<sup>2</sup>, Jean Canou<sup>2</sup>

1: Zhejiang University, China

2: Laboratoire Navier/CERMES, Ecole des Ponts ParisTech (ENPC), France

3: Department of Civil and Environmental Engineering, The Hong Kong Polytechnic  
University, Hung Hom, Kowloon, Hong Kong, China

**Corresponding author:**

Mr. Shuai Qi  
Department of Civil Engineering  
Zhejiang University, Hangzhou, China  
E-mail: [qishuailw@163.com](mailto:qishuailw@163.com)

## Abstract

Ballast/fines mixture is often found in railway substructure and the overall behaviour of tracks is strongly dependent on the mechanical behaviour of this mixture. Since directly testing such mixture with large grains is limited with common laboratory equipment, the consideration of a model material at smaller size is advisable. Parallel gradation method is widely used for this purpose. This study assesses the validity of this method in the case of ballast/fines mixture. Large-scale cyclic triaxial tests were carried out on the ballast/fines mixture at six volumetric coarse grain contents. The results obtained were analysed, together with those obtained previously from small-scale triaxial tests on a microballast/fines mixture whose microballast grain size distribution was determined by applying the parallel gradation method. The cyclic parameters (permanent strain and resilient modulus) were obtained for the two types of mixture. Results show that for all mixtures two distinct soil fabrics can be identified according to the variations of permanent strain and resilient modulus with the volumetric content of coarse grains  $f_v$ : a fine-fine contact structure for  $f_v \leq 20\%$  and a grain-grain contact structure for  $f_v \geq 35\%$ . In the case of fine-fine contact structure, the permanent strains and resilient modulus values of the ballast specimens are consistent with those of the microballast specimens, evidencing the validity of the parallel gradation method. In the case of grain-grain contact structure, the permanent strains and resilient modulus values are found to coincide globally at the two scales, also justifying the validity of the parallel gradation method, the slight differences between the two scales being attributed to the irregular grain sliding and the

45 distribution of the fines soils.

46

47 **Keywords:** interlayer soil; cyclic triaxial tests; permanent deformation; resilient

48 modulus; parallel gradation method

## 1. Introduction

Ballast/fines mixture is often found in railway substructure [10,17]. For instance, in the French conventional railway lines (representing 94% of the total railway network), there is an interlayer which was formed by interpenetration of ballast and subgrade soils under the effect of train circulation [10]. During the renewable program for conventional lines, this layer was maintained since the dry density of the interlayer was as high as  $2.4 \text{ Mg/m}^3$  and thus a favourable mechanical behaviour was expected [7]. According to the in-situ investigation, the soil fabric of the interlayer is found to be greatly dependent on the content of ballast grains [37,38]: the ballast grains are in contact with each other for the upper part with high ballast content, but floated in the fines matrix for the lower part with lower ballast content. Since the ballast/fines mixture plays an important role in the overall behaviour of rail tracks, it is important to investigate the mechanical response of such mixture under cyclic loading in terms of permanent deformation and resilient modulus. Considering the large size of ballast grains, large-scale triaxial apparatus is normally needed for this purpose. However, since the large testing system is complex and costly, scaling the ballast grains down to a model ballast material with smaller size and performing tests using standard apparatus appear quite promoting.

Three methods are commonly used for the scaling purpose: the scalping method [50] which consists in discarding the grains larger than a specified size from the prototype materials, the parallel gradation method [24] which consists in creating a model material at smaller size with its grain size distribution parallel to that of the

prototype material, and the replacement method [14] which consists in replacing the grains from a specified size to the maximum size with the grains from this specified size to a smaller size. Among them, the parallel gradation method is regarded to be the most appropriate because it can consider a large range of prototype gradation shape; thus, it has been adopted mostly [1,16,29,39,42,43,44,47]. The validity of this method under cyclic loadings was assessed by Sevi and Ge [34] based on the response of the prototype and model grains of ballast grains. Their results in terms of resilient modulus, permanent axial strain and permanent volumetric strain were unfortunately not conclusive for validating the parallel gradation method. In addition, only pure ballast grains were tested without fines fraction.

In this study, the parameters characterizing the cyclic response (permanent strain and resilient modulus) of ballast/fines mixtures representing the interlayer soils in the conventional French railway track-beds were determined by conducting large-scale cyclic triaxial tests. Six volumetric ballast contents (0%, 5%, 10%, 20%, 35%, 45%) were considered. The results obtained were analysed together with those obtained previously by Wang et al. [42,43] from small-scale cyclic triaxial tests on microballast/fines mixture with microballast prepared by applying the parallel gradation method. Comparison of the mechanical parameters obtained at two scales allowed the validity of the parallel gradation method to be assessed on coarse grain/fines mixtures.

## 2. Materials

The ballast grains having the same grain size distribution as the interlayer soil in “Sénissiat site” were used [37], as shown in Fig. 1. The minimum grain size  $D_{\min}^b$  and the maximum grain size  $D_{\max}^b$  are 20 mm and 63 mm, respectively. The microballast was tested previously by Wang et al. [42,43]; its maximum grain size  $D_{\max}^m$  was chosen as 20 mm to adapt to a small-scale triaxial cell of 100 mm with a value of 5 as the ratio of specimen to maximum grain size. This is consistent with the recommendation of Fagnoul and Bonnechere [12], Nitchiporovitch [25] and Pedro [28]: a ratio larger than 5 must be adopted to minimize the specimen size effect. The grain size distribution of the microballast is transited from that of the ballast by following the parallel gradation method. In this method, the correlative grain sizes of ballast and microballast share the same percentage of grain passing. The grain sizes of these two materials are correlated according to the following equation:

$$(1) \quad \frac{D^b - D_{\min}^b}{D^m - D_{\min}^m} = \frac{D_{\max}^b - D_{\min}^b}{D_{\max}^m - D_{\min}^m} = A$$

where  $D_{\max}$ ,  $D_{\min}$  and  $D$  are the maximum grain size, the minimum grain size, and a given grain size, respectively. The superscripts  $b$  and  $m$  stand for ballast and microballast, respectively.  $A$  is a constant.

To prepare the microballast, three angular-shaped commercial coarse grains were used. Visually, the grain shape of the chosen commercial grains was similar to that of the field ballast from “Sénissiat site”. The minimum grain size of the commercial grains  $D_{\min}^m$  was 1.6 mm, defining a value of 2.337 for parameter  $A$ . For a given grain size of microballast  $D^m$ , 10.0 mm for instance, equation (1) gives a

correlated ballast grain size  $D^b$  of 39.6 mm. As the ballast grain passing percentage is 59.1 % for  $D^b = 39.6$  mm, according to the parallel gradation method, the microballast grain passing percentage is also 59.1 % for  $D^m = 10$  mm. Following this procedure, the complete grain size distribution of the microballast was obtained, as shown in Fig. 1. This target (parallel gradation) curve was verified by measurement and it is observed that the measured grain size distribution and the target one show a good agreement (Fig. 1).

For the fines soils, since obtaining enough quantity from the field was difficult, they were fabricated in the laboratory. Nine commercial soils were mixed to simulate the fines soils from “Sénissiat site”, which included five kinds of medium sands, two kinds of fine sands and two kinds of clay soils (kaolinite and bentonite). Table 1 listed the properties of these soils. The mass proportion of each constituting soil was calculated according to the grain-size distributions of the fines from “Sénissiat site” (Fig. 2). The calculated results were also shown in Table 1. With the proportion and the grain size distribution of each soil, the grain size distribution of the fabricated fines can be calculated, which was plotted in Fig. 2 as well. During the mixing procedure, the materials to be mixed were carefully added into the mixer following the sequence of medium sands, water, fine sands, kaolinite and bentonite. The mass of the added water corresponded to a small water content of 4% of the total mixed soils. The aim of water addition was to prevent the small particles loss during the mixing, occurring when fine sands, kaolinite and bentonite were dry mixed with others. Bentonite was added last since it was the most reactive soil with water. With this



sequence, most kaolinite and bentonite particles were expected to be adhered to the surface of sands. Using this procedure, a homogeneous mixture can be obtained [21]. Wang et al. [42,43] also adopted this method when preparing specimens of microballast and fines mixture. After preparation, the fabricated fines soil was compared with the field one in terms of grain size distribution and plasticity. As can be observed from Fig. 2, the grain size distribution of the fabricated fines showed a good agreement with that of the in situ one. In addition, the liquid limit and the plasticity index of the fabricated fines, which were 32% and 20%, respectively, matched the target liquid limit (35.5%) and plasticity index (17.3%) well. This soil is classified as lean clay (CL) according to ASTM D2487-11 [3]. Standard Proctor compaction tests were carried out on the fines material following ASTM D698-12 [4]. An optimum water content  $w_{\text{opt-f}} = 13.70\%$  and a maximum dry density  $\rho_{\text{dmax-f}} = 1.82 \text{ Mg/m}^3$  were determined.

### **3. Experimental methods**

#### **3.1. Specimen preparation**

In order to quantify the coarse grains in a specimen, a parameter namely volumetric content of coarse grains  $f_v$  was adopted, which was defined as the ratio of the total volume of coarse grains to the total specimen volume [28,29,32,42,43,44]. The total specimen volume consisted of two parts: the coarse grain volume and the fines volume. All pores were assumed to be included in the fines soils. For the upper part of the natural interlayer soils at “Sénissiat site”, the  $f_v$  value was 52.9% [37]. In this

study, six  $f_v$  values (0%, 5%, 10%, 20%, 35%, 45%) were considered for the specimens prepared with both ballast and microballast. For convenience, in further analysis, the specimens prepared with ballast and microballast are referred to as ballast specimens and microballast specimens, respectively. The dimensions of the ballast specimens are 300 mm diameter and 600 mm height, while the dimensions of microballast specimens are 100 mm diameter and 200 mm height.

For the preparation of the ballast specimen, the total volume was first calculated with the specimen dimensions (300 mm diameter and 600 mm height). For a given  $f_v$  value, the volumes of both ballast grains and fines can be obtained based on this total specimen volume. After that, the mass of ballast was obtained using the dry unit mass of ballast (2.68 Mg/m<sup>3</sup>). The fines in all specimens were kept at the same state defined by the optimum water content  $w_{\text{opt-f}} = 13.70\%$  and the maximum dry density  $\rho_{\text{dmax-f}} = 1.82 \text{ Mg/m}^3$ . The optimum state was selected aiming to simulate the heavily compact state in the field condition [8,21,38]. Accordingly, the masses of dry fines and water can be determined. Water was firstly added into the fines by spray to reach the optimum water content  $w_{\text{opt-f}} = 13.7\%$ . Then, the wetted fines soil was stored in hermetic containers for 24 h for moisture homogenization. Afterwards, the homogenized wetted fines soil was equally divided into eight parts (by weight) and so were the oven-dried ballast grains, after which they were mixed separately. Finally, the ballast specimen was compacted using a layered compaction method, which was widely adopted by many researchers to ensure reasonable uniformity of the specimen [5,22,35,46]. The mixed materials were compacted in eight layers using a vibration

hammer, each with a thickness of 75 mm.

Similar protocol was applied for the preparation of the microballast specimen (100 mm diameter and 200 mm height). The masses of the dry microballast, dry fines soil and water were firstly determined. Afterwards, the fines soil was wetted with the sprayed water to reach the optimum water content of 13.7%, stored in hermetic container for 24 h and then mixed with the microballast. Finally, this mixture was compacted dynamically to reach the target height, also following the layered compaction method to ensure reasonable uniformity of the specimen. More details can be found in Wang et al. [42,43]. Note that the test results at five  $f_v$  values (5%, 10%, 20%, 35%, 45%) obtained by Wang et al. [42,43] were taken for comparison with the corresponding ones of the ballast samples in this study.

### **3.2. Cyclic triaxial tests**

For the microballast specimen with 100 mm diameter and 200 mm height, a small-scale cyclic triaxial apparatus was used. Details about this device can be found in Wang et al. [43]. For testing a ballast specimen (300 mm diameter and 600 mm height), a large-scale cyclic triaxial apparatus developed by Dupla et al. [11] was adopted. The loading procedures adopted are the same for the ballast and the microballast specimens. No saturation process was applied and the specimen water content was kept constant during the test. In addition, the drainage valve was kept open during the loading process. All the tests were performed at a confining pressure of 30 kPa, which corresponded to the average horizontal stress estimated for the field

condition, considering the effects of the train wheel load, the interlayer depth and the Poisson ratio [9,42,43]. The applied cyclic loads followed a sine-shaped pattern (Fig. 3). The deviator stress amplitude  $\Delta q$  is defined as the difference value between the maximum deviator stress  $q_{max}$  and the minimum deviator stress  $q_{min}$  [40,41,42,43]. A frequency of 1.78 Hz corresponding to a low train speed of 50 km/h was chosen, aiming to guarantee the quality of controlling the pre-defined loading shape. Note that this low frequency did not reflect the high train speed normally encountered in the field. This selection was based on the hypothesis that the train speed does not influence the assessment of the validity of the parallel gradation. During the loading procedure, axial stress and strain were monitored.

The application of cyclic loads included two consecutive stages. The loading stage 1 was focused on the aspect of the permanent deformation under a large number of loading cycles. The loading stage 2 was focused on the aspect of the resilient modulus or stiffness property under a wide range of stress amplitudes, including some large amplitudes possibly applied on the interlayer soils. In stage 1, a multi-step loading procedure proposed by Gidel et al. [13] was adopted (Fig. 4a): the deviator stress amplitude  $\Delta q = q_{max} - q_{min}$  was increased stepwise from 10 kPa to 30 kPa with an increment of 5 kPa. At each amplitude, 90,000 cycles were applied, which were thought to be enough for the stabilization of the permanent strain [10,13,21,38]. This multi-stage loading procedure allowed the application of several stress amplitudes on the same specimen, with which not only the number of tests could be reduced, but also the effect of the variability of soil specimens on the testing results can be

minimised. Thus, this procedure has been widely used in the study of the permanent deformation behaviour [6,10,19,21,36,38,43]. These loading amplitudes were selected based on the vertical stress measured at the equivalent depth of interlayer in the field [20,21]. In stage 2 (Fig. 4b), a procedure proposed by Lamas-Lopez [23] was adopted. The deviator stress amplitude  $\Delta q$  was firstly increased following a  $\Delta q$  sequence (10 kPa, 30 kPa and 50 kPa) and then decreased following the reverse sequence. Afterwards,  $\Delta q$  was increased following a sequence from 10 kPa to 100 kPa and then decreased to 10 kPa. Finally,  $\Delta q$  was increased in steps to 200 kPa and then decreased to 10 kPa. At each stress level, 100 cycles were applied. The aim of firstly increasing  $\Delta q$  and then decreasing it was to obtain the resilient modulus at both elastoplastic stage and pure elastic stage. Note that the large stress amplitudes (50 kPa, 100 kPa and 200 kPa) were defined according to the vertical stress of 40-90 kPa at similar depth of the interlayer observed by Selig and Waters [33], Jain and Keshav [18] and Yang et al. [49], the vertical stress of 120-138 kPa applied by heavier wagons in some countries [15,18,23] and the contingent maximum vertical stress at the top of railway structure as high as 200 kPa [21].

## 4. Results and discussions

### 4.1. Variations of permanent deformation with $f_v$

Fig. 5 plots the deviator stress  $q$  versus the axial strain  $\varepsilon_1$  during the first 90,000 cycles of loading stage 1 for the ballast specimen at  $f_v = 35\%$ . In a loading-unloading cycle, the permanent axial strain  $\varepsilon_{1p}$  represented the irreversible part of the total

axial strain. It can be observed that the  $\varepsilon_{1p}$  value of the first cycle was particularly large. This phenomenon was also observed for other ballast specimens and the microballast specimens. This large permanent strain can be attributed to the adaptation of the specimen to the loading system, in particular in terms of contact between the specimen and the loading piston. As the initial specimen-piston contact was not identical for all the specimens, this  $\varepsilon_{1p}$  value would make impossible the relevant comparison of permanent strain between different specimens. Thus, in further analysis, the first cycle was not accounted for the cumulative permanent strain.

Fig. 6 presents the permanent strain  $\varepsilon_{1p}$  against the number of cycles  $N$  for six ballast specimens, with the corresponding stress levels. The evolutions of permanent strain with number of cycles  $N$  were the same as the ones of microballast specimens [43]. It can be observed from Fig. 6 that for each  $f_v$  value,  $\varepsilon_{1p}$  increased quickly at the start of each loading level and then tended to stabilize with the increasing cycles. According to Werkmeister et al. [45], the large deformation in the beginning resulted from a significant rearrangement of the particles. As the cycle number increased, this particle rearrangement became more and more limited, and correspondingly, the permanent strain tended to become stable. As can also be seen from Fig. 6, a smaller  $f_v$  value led to a larger  $\varepsilon_{1p}$ , which can be attributed to the involvement of less coarse grains.

Due to the multi-step loading procedure adopted, the  $\varepsilon_{1p}$  at each stress level was greatly influenced by the previous loadings (Fig. 6). If this loading history is eliminated (as if the specimen has been subjected to only one loading level), the effect

of the ballast contents can be better evaluated. For this purpose, a permanent strain estimation method proposed by Gidel et al. [13] and then used by Lamas-Lopez [21] and Wang et al. [43] was adopted. The application of this method is explained in Fig. 7 by considering two successive loading levels (Loading level  $M$  and Loading level  $M + 1$ ). For the estimated permanent strain  $\varepsilon_{1p}^{M+1}$  of the Loading level  $M + 1$  at the first 90,000 cycles, it is determined as:

$$(2) \quad \varepsilon_{1p}^{M+1} = \varepsilon_{1p}^M + \delta\varepsilon_{1p}^{M+1}$$

where  $\varepsilon_{1p}^M$  is the measured permanent strain of the Loading Level  $M$ ;  $\delta\varepsilon_{1p}^{M+1}$  is the translated permanent strain determined by resetting both the initial strain value and the first cycle of the measured permanent strain of the Loading level  $M + 1$  to 0.

For estimating the permanent strain of the Loading level  $M + 1$  after 90,000 cycles, a linear increasing trend between permanent strain and number of cycles is considered, with its slope kept at the same value as the one determined at the last cycles of Loading level  $M + 1$ . More details can be found in Wang et al. [43].

The estimated permanent strain curves for  $f_v = 0\%$  of the ballast specimen are presented in Fig. 8, together with the measured results. It can be observed that at the last cycle of each stress level, the estimated strain was larger than the measured one. For example, for  $\Delta q = 20$  kPa, the measured permanent strain at the last cycle  $N = 270,000$  was 0.182%, while the corresponding estimated one was 0.226%. This phenomenon can be attributed to the different loading histories: for the estimated strain, the specimen was assumed to undergo one higher stress level of 20 kPa. When it came to the measured strain, successive lower stress levels of 10kPa, 15 kPa and 20

kPa were applied, leading to a smaller strain value.

Gidel et al. [13] examined this permanent strain estimation method through cyclic triaxial tests, concluding that the permanent strain estimated for a single stress level agreed well with the measured one for the loading cycles applied at each step (90,000 cycles in this study). In other words, in this study, the estimated permanent strain at the first 90,000 cycles was relatively accurate. Fig. 9 depicts the estimated permanent strain evolutions at the first 90,000 cycles under different stress levels for ballast specimen at  $f_v = 0\%$ . As can be observed, a larger stress level led to a larger strain value. In addition, the permanent strain gradually stabilized with the increase of the cycle number. To further illustrate the effect of ballast content  $f_v$ , the estimated permanent strains for cycle  $N = 90,000$  (end-stage cycle in Fig. 9) at all stress levels were taken and compared (Fig. 10). It can be observed that at each stress level, the permanent strain decreased with the increase of  $f_v$ . Moreover, a bi-linear decreasing trend could be identified. When  $f_v \leq 20\%$ , the permanent strain decreased rapidly. By contrast, when  $f_v \geq 35\%$ , this decreasing rate became smaller. The same observations were made by Wang et al. [43] for the microballast specimens.

In the study of Wang et al. [43], X-ray microcomputed tomography ( $\mu$ CT) scans were carried out on the as-compacted microballast specimens. Two soil fabrics were identified at different  $f_v$  values: a fine-fine contact structure at  $f_v = 0\%$ -20% and a distinct grain-grain contact structure at  $f_v = 35\%$ -45%. It is worth noting that at  $f_v = 20\%$ , the coarse grains started to be partially connected without forming a whole skeleton. Unfortunately, this  $\mu$ CT scan could not be conducted on ballast specimens



due to their large size. However, basically, it seems plausible to consider the same feature of fabrics for the ballast specimens: also a fine-fine contact structure at low  $f_v$  and a grain-grain contact structure at high  $f_v$ . For fine-fine contact structure, the permanent strain results from the compression of the fines, which decreases rapidly with increasing  $f_v$ . By contrast, for grain-grain contact structure, the rearrangement of the grains plays a dominant role and the permanent strain decreases slightly when  $f_v$  increases.

#### **4.2. Variations of resilient modulus with $f_v$**

Typical hysteresis loops at the first cycles of different stress levels are shown in Fig. 11 for the ballast specimen at  $f_v = 20\%$ . The loops for stress levels of  $\Delta q = 10$  kPa,  $\Delta q = 30$  kPa,  $\Delta q = 50$  kPa,  $\Delta q = 100$  kPa and  $\Delta q = 200$  kPa corresponded to cycle numbers of  $N = 1$ ,  $N = 101$ ,  $N = 201$ ,  $N = 701$  and  $N = 1401$ , respectively. It appears that for the low stress levels of 10 kPa and 30 kPa, the hysteresis loops were pretty small and closed. This was due to the application of 450,000 loading cycles under  $\Delta q \leq 30$  kPa in loading stage 1. By contrast, for stress levels larger than 30 kPa, permanent strain developed, leading to larger and unclosed hysteresis loops, in particular under stress levels as high as  $\Delta q = 100$  kPa and 200 kPa.

The evolution of hysteresis loop with number of cycles is illustrated in Fig. 12 by plotting the loops for 100 cycles (from  $N = 701$  to  $N = 800$ ) at  $\Delta q = 100$  kPa for the ballast specimen with  $f_v = 20\%$ . A large and unclosed hysteresis loop was observed for the first cycle, due to the stress level of 100 kPa which was larger than all the

previous applied stress levels. In addition, with the increase of the cycle number, the hysteresis loop became smaller and smaller and at the end of loading, the loops became closed and relatively unchanged, suggesting a pure elastic behaviour of soil.

As shown in Fig. 13, the resilient modulus  $M_r$  is defined as [30,31]:

$$(3) \quad M_r = \Delta q / \varepsilon_{1r}$$

where  $\Delta q$  is the deviator stress amplitude, and  $\varepsilon_{1r}$  is the resilient strain.

The evolution of  $M_r$  with the number of cycles  $N$  at varying stress levels is presented in Fig. 14 for the ballast specimen at  $f_v = 20\%$ . The results of other ballast specimens and microballast specimens obey the same rule and are not shown for clarity. It can be observed that when the stress amplitude increased, the  $M_r$  value immediately decreased and then tended to stabilize. By contrast, with the stress amplitude decreasing, the  $M_r$  value increased instantly and then tended to reach a stabilization state. The decrease of  $M_r$  with the increase of stress amplitude can be explained by the strain increasing due to the increase of stress amplitude [2].

In order to illustrate the effect of  $f_v$  on resilient modulus, the  $M_r$  values of the last (end-stage) cycles of all stress levels were taken and presented as a function of  $f_v$  for different stress levels (Fig. 15). The data were named according to the number of cycles  $N$  and the corresponding  $\Delta q$  values. It appears that an increasing trend of  $M_r$  with  $f_v$  can be identified for all stress levels. Moreover, this increasing trend followed a bi-linear pattern with the slope at  $f_v \geq 35\%$  larger than the one at  $f_v \leq 20\%$ , evidencing that the soil fabrics of the ballast specimens at these two  $f_v$  ranges were different: fine-fine contact structure at low  $f_v$  and grain-grain contact structure at

higher  $f_v$ . Same bi-linear variation trend of  $M_r$  was identified by Wang et al. [42] for the microballast specimens, similarly, evidencing that the soil fabrics of microballast specimens at  $f_v \leq 20\%$  and  $f_v \geq 35\%$  were separately dominated by fine-fine contact structure and grain-grain contact structure.

#### **4.3. Comparison of permanent strain between ballast and microballast specimens**

The estimated permanent strains for cycle  $N = 90,000$  (end-stage cycle) at six  $f_v$  values are presented in Fig. 16 for the ballast and the microballast specimens, for five stress levels (10, 15, 20, 25 and 30 kPa). It can be observed that in the case of  $f_v = 0\%$ , at each stress level, the  $\varepsilon_{1p}$  value of the ballast specimen coincides well with that of the microballast specimen. For the fine-fine contact structure at  $f_v = 5\%$  and  $10\%$ , on the whole, the  $\varepsilon_{1p}$  values of the corresponding different scale specimens are found to be similar. This phenomenon can be explained by the fact that in this case the fines matrix constitutes the soil skeleton and the permanent strain was dominated by the compression of the fines, giving rise to the permanent strains which were independent of coarse grain size. For the grain-grain contact structure at  $f_v = 35\%$  and  $45\%$ , it can be observed that the permanent strains of the ballast specimens and the microballast specimens were almost the same (Fig. 16), in particular at  $\Delta q = 10$  kPa (Fig. 16a). Note that although the case at  $f_v = 20\%$  was categorized into the group of fine-fine contact structure, the influence of coarse grain size on the permanent strain followed the same pattern. This can be explained by the fact that at  $f_v = 20\%$ , part of the coarse

grains started to be in contact with each other. Further examination shows that at  $\Delta q$  higher than 10 kPa, the strains of microballast specimens were slightly larger than those of the ballast specimens. This phenomenon can be explained as follows: upon loadings, the grains would slide into the pores nearby, giving rise to permanent strain. If the difficulty of sliding into large pores for the large grains was the same as that for the smaller grains to slide into smaller pores, identical permanent strains can be expected. It is the case for the ballast specimen and the microballast specimen at  $\Delta q = 10$  kPa. Apparently, the grains sliding depended on the stress level and the grain sizes; in the microballast specimen, the grains with smaller sizes would slide into the adjacent pores more easily, leading to a slightly larger strain.

Another possible explanation for the slightly larger strains in the microballast specimen is related to the effect of the fines soils. As shown in Fig. 17, the fines soils can be roughly considered to be distributed at two locations: the pores near the coarse grain and the coarse grain intervals along the stress chain (supposed to be along the specimen height). The applied load was transmitted along the stress chain by compressing the fines between grains. When the load reached a certain level, grain rearrangement occurred [26,27]. It can be inferred that the fines in the pores inhibited the coarse grain sliding, while those between grains promoted it. At a given  $f_v$  value, for the microballast specimen, more grain-fines-grain contacts can be expected along the stress chain, leading to more distribution of fines soils. As a result, relatively larger permanent strain can be expected.

As the difference of permanent strain between the two scale specimens appears

quite small (Figure. 16), it can be reasonably concluded that the parallel gradation method is valid for the ballast/fines mixture in terms of permanent strain.

#### **4.4. Comparison of resilient modulus between ballast and microballast specimens**

The comparison of  $M_r$  values between the microballast and ballast specimens with fine-fine contact structure is shown in Fig. 18. At  $f_v = 0\%$ , the  $M_r$  values of the ballast specimen were comparable with those of the microballast specimen. This was normal because the scaling question was not involved in that case. For higher  $f_v$  values, except  $f_v = 10\%$ , the  $M_r$  values of the ballast and the microballast specimens coincided with each other. The singular case at  $f_v = 10\%$  was probably due to a technical problem.

The  $M_r$  values of the ballast specimens at grain-grain contact structure were compared with those of the microballast specimens in Fig. 19 (Fig. 19a for  $f_v = 35\%$  and Fig. 19b for  $f_v = 45\%$ ). It can be observed that almost the same  $M_r$  values were obtained for the two specimens, indicating that the resilient modulus was independent of grain size. Further investigation shows that on the whole the  $M_r$  values of the microballast specimens were slightly smaller than those of the ballast specimens. These phenomena can be explained based on the analysis of Yang and Gu [48]. They derived the resilient modulus of a simple cubic array of identical spheres under a certain confining pressure by applying a small shear stress onto it. In the analysis, the induced resilient shear strain of the cubic array was determined by adding up the tangential strains between every two spheres along the vertical stress chain. This tangential strain was calculated using the Hertz-Mindlin contact law, which was a

function of the applied shear stress. The expression for the resilient modulus (defined as the ratio of the shear stress to the shear strain) was obtained, showing no dependence on sphere radius. Note that this analysis did not consider any contribution from fine soils, thus not fully reflecting the case of this study. Indeed, as mentioned previously, in the case of mixture, the resilient modulus is affected by the fine soils along the stress chain. For the microballast specimens, as stated before, there are more fines soils along it. Thus, relatively smaller resilient modulus values are expected.

As for the permanent strain, globally, the resilient modulus also showed a good agreement between the two scale specimens albeit the slight difference discussed above, which validates the parallel gradation method in terms of resilient modulus.

## **5. Conclusions**

The parallel gradation method was assessed on coarse grain/fines mixture by comparing the mechanical parameters (permanent strain and resilient modulus) of the two different scale specimens. Six volumetric coarse grain contents were considered for each kind of specimens. Based on the results obtained, the following conclusions can be drawn.

Two soil fabrics could be defined as fine-fine contact structure at  $f_v = 0-20\%$  and grain-grain contact structure at  $f_v = 35-45\%$ . It was observed that for the ballast and microballast specimens, with the increase of  $f_v$  value, the permanent strain decreased rapidly when  $f_v \leq 20\%$  and this decreasing rate slowed down when  $f_v \geq 35\%$ , while the resilient modulus increased slightly when  $f_v \leq 20\%$  and increased

significantly when  $f_v \geq 35\%$ .

The consistency between the large-scale and small-scale triaxial tests were found to be satisfactory: at  $f_v = 0\%$ , the permanent strain as well as the resilient modulus values obtained from the two scales showed a good correspondence. In the case of fine-fine contact structure, the parallel gradation method was found to be valid. The permanent strain and resilient modulus values of the ballast specimens were consistent with the respective ones of the microballast specimens. This could be explained by the fact that in this case the fines matrix governed the soil structure.

In the case of grain-grain contact structure, on the whole, the permanent strains of the ballast specimens coincided with those of the microballast specimens (especially at  $\Delta q = 10$  kPa). This coincidence was also observed in terms of resilient modulus. For the permanent strain, it could be explained by the fact that the difficulties of the sliding of large ballast grains into the adjacent large pores and the sliding of the small microballast grains into the smaller pores were expected to be the same. For the resilient modulus, it could be explained by the analytical results of Yang and Gu (2013), showing that the resilient modulus is independent of grain size. Further examination showed that there were slight differences of permanent strain and resilient modulus between two different scale specimens, which could be attributed to the irregular grain sliding and the fines distribution.

#### **Acknowledgements**

The support from the Chinese Scholar Council (CSC) is greatly acknowledged.

467 **Notations**

$A$	constant in the similitude equation from ballast to microballast
$D^b$	given grain size of ballast
$D_{\max}^b$	maximum grain size of ballast
$D_{\min}^b$	minimum grain size of ballast
$D^m$	given grain size of microballast
$D_{\max}^m$	maximum grain size of microballast
$D_{\min}^m$	minimum grain size of microballast
$f_v$	volumetric content of coarse grains
$M_r$	resilient modulus
$N$	number of cycles
$q$	deviator stress
$q_{\max}$	maximum deviator stress
$q_{\min}$	minimum deviator stress
$w_{\text{opt-f}}$	optimum water content of fines
$\Delta q$	deviator stress amplitude
$\delta \varepsilon_{1p}^{M+1}$	translated permanent strain from the measured curve of Loading level M+1
$\varepsilon_1$	axial strain



$\varepsilon_{1p}$	permanent axial strain
$\varepsilon_{1r}$	resilient strain
$\varepsilon_{1p}^M$	measured permanent strain of the Loading Level $M$
$\varepsilon_{1p}^{M+1}$	estimated permanent strain of Loading level $M+1$
$\rho_{\text{dmax-f}}$	maximum dry density of fines

468

## 469 **References**

- 470 [1] Aingaran, S. 2014. Experimental investigation of static and cyclic behavior of  
471 scaled railway ballast and the effect of stress reversal. Ph.D. thesis, University of  
472 Southampton.
- 473 [2] Atkinson, J.H. 2000. Non-linear soil stiffness in routine design. *Géotechnique*,  
474 50(5): 487-507.
- 475 [3] ASTM. 2011. D2487-11: Standard practice for classification of soils for  
476 engineering purposes (unified soil classification system). ASTM International,  
477 West Conshohocken, PA, USA.
- 478 [4] ASTM. 2012. D698-12: Standard test methods for laboratory compaction  
479 characteristics of soil using standard effort. ASTM International, West  
480 Conshohocken, PA, USA.
- 481 [5] Cai, Y.Q., Chen, J.Y., Cao, Z.G., Gu, C., and Wang, J. 2018. Influence of grain  
482 gradation on permanent strain of unbound granular materials under low confining  
483 pressure and high-cycle loading. *International Journal of Geomechanics*, 18(3):  
484 04017156.

- 485 [6] Cao, Z.G., Chen, J.Y., Cai, Y.Q., Zhao, L., Gu, C., and Wang, J. 2018. Long-term  
486 behavior of clay-fouled unbound granular materials subjected to cyclic loadings  
487 with different frequencies. *Engineering Geology*, 243: 118-127.
- 488 [7] Cui, Y.J., Duong, T.V., Tang, A.M., Dupla, J.C., Calon, N., and Robinet, A. 2013.  
489 Investigation of the hydro-mechanical behavior of fouled ballast. *Journal of*  
490 *Zhejiang University-Science A (Applied Physics & Engineering)*, 14(4): 244-255.
- 491 [8] Duong, T.V. 2013. Investigation of the hydro-mechanical behavior of ancient  
492 railway platforms in scope to reinforcement by soil-mixing. Ph.D. thesis, Ecole  
493 Nationale des Ponts et Chaussées, Université Paris-Est.
- 494 [9] Duong, T.V., Cui, Y.J., Tang, A.M., Dupla, J.C., Canou, J., Calon, N., and Robinet,  
495 A. 2016. Effects of water and fines contents on the resilient modulus of the  
496 interlayer soil of railway substructure. *Acta Geotechnica*, 11(1): 51-59.
- 497 [10] Duong, T.V., Tang, A.M., Cui, Y.J., Trinh, V.N., Dupla, J.C., Calon, N., Canou, J.,  
498 and Robinet, A. 2013. Effects of fines and water contents on the mechanical  
499 behavior of interlayer soil in ancient railway sub-structure. *Soils and Foundations*,  
500 53(6): 868-878.
- 501 [11] Dupla, J.C., Pedro, L.S., Canou, J., and Dormieux, L. 2007. Mechanical behavior  
502 of coarse grained soils reference. *Bulletin de Liaison des Laboratoires des Ponts*  
503 *et Chaussées*, 268-269: 31-58.
- 504 [12] Fagnoul, A., and Bonnechere, F. 1969. Shear strength of porphyry materials. *In*  
505 *Proceedings of the 7th International Conference on Soil Mechanics and*  
506 *Foundation Engineering*, Mexico, pp. 61-65.

- 507 [13] Gidel, G., Hornych, P., Chauvin, J.J., Breysse, D., and Denis, A. 2001. A new  
508 approach for investigating the permanent deformation behavior of unbound  
509 granular material using the repeated load triaxial apparatus. *Bulletin des*  
510 *Laboratoires des Ponts et Chaussées*, 233: 5-21.
- 511 [14] Frost, R.J. 1973. Some testing experiences and characteristics of boulder-gravel  
512 fills in earth dams. *In* Evaluation of relative density and its role in geotechnical  
513 projects involving cohesionless soils. STP 523. ASTM Standards and  
514 Publications.
- 515 [15] Grabe, P., and Clayton, C. 2009. Effects of principal stress rotation on permanent  
516 deformation in rail track foundations. *Journal of Geotechnical and*  
517 *Geoenvironmental Engineering*, 135(4): 555–565.
- 518 [16] Indraratna, B., Wijewardena, L.S.S., and Balasubramaniam, A.S. 1993.  
519 Large-scale triaxial testing of greywacke rockfill. *Géotechnique*, 43: 37-51.
- 520 [17] Indraratna, B., Su, L., and Rujikiatkamjorn, C. 2011. A new parameter for  
521 classification and evaluation of railway ballast fouling. *Canadian Geotechnical*  
522 *Journal*, 48(2): 322-326.
- 523 [18] Jain, V., and Keshav, K. 1999. Stress distribution in railway formation - a  
524 simulated study. *In* Proceeding of the 2<sup>nd</sup> International Symposium on Pre-Failure  
525 Deformation Characteristics of Geomaterials-IS Torino.
- 526 [19] Jing, P., Nowamooz, H., and Chazallon, C. 2016. Permanent deformation  
527 behaviour of a granular material used in low-traffic pavements. *Road Materials*  
528 *and Pavement Design*, 19(2): 289-314.

- 529 [20] Lamas-Lopez, F., Costa D'Aguiar, S., Robinet, A., Cui, Y.J., Calon, N., Canou, J.,  
530 Dupla, J.C., and Tang, A.M. 2015. In-situ investigation of the behaviour of a  
531 French conventional railway platform. *In* Proceedings of Transportation Research  
532 Board TRB 2015, Washington, DC.
- 533 [21] Lamas-Lopez, F. 2016. Field and laboratory investigation on the dynamic  
534 behaviour of conventional railway track-bed materials in the context of traffic  
535 upgrade. Ph.D. thesis, Ecole Nationale des Ponts et Chaussées, Université  
536 Paris-Est.
- 537 [22] Lenart, S., Koseki, J., Miyashita, Y., and Sato, T. 2014. Large-scale triaxial tests  
538 of dense gravel material at low confining pressures. *Soils and Foundation*, 54(1):  
539 45-55.
- 540 [23] Li, D., and Selig, E. 1998. Method for railroad track foundation design. I:  
541 Development. *Journal of Geotechnical and Geoenvironmental Engineering*,  
542 124(4): 316–322.
- 543 [24] Lowe, J. 1964. Shear strength of coarse embankment dam materials. *In*  
544 *Proceedings of the 8th International Congress on Large Dams 3*, Edinburgh, U.K.,  
545 pp. 745-761.
- 546 [25] Nitchiporovitch, A.A. 1969. Shearing strength of coarse shell materials. *In*  
547 *Proceedings of the 7th International Conference on Soil Mechanics and*  
548 *Foundation Engineering*, Mexico, pp. 211-216.
- 549 [26] Oda, M., Konishi, J., and Nasser, N.S. 1982. Experimental micromechanical  
550 evaluation of strength of granular materials: effects of particle rolling. *Mechanics*

551 of Materials, 1(4): 269-283.

552 [27] Oda, M., and Kazama, H. 1998. Microstructure of shear band and its relation to  
553 the mechanisms of dilatancy and failure of dense granular soils. *Géotechnique*,  
554 48(4): 465-481.

555 [28] Pedro, L. 2004. De l'étude du comportement mécanique de sols hétérogènes  
556 modèles à son application au cas des sols naturels. Ph.D. thesis, Ecole Nationale  
557 des Ponts et Chaussées, Université Paris-Est.

558 [29] Qi, S., Cui, Y.J., Chen, R.P., Wang, H.L., Lamas-Lopez, F., Aïmedieu, P., Dupla,  
559 J.C., Canou, J., and Saussine, G. 2019. Influence of grain size distribution of  
560 inclusions on the mechanical behaviors of track-bed materials. *Géotechnique* in  
561 press. doi : 10.1680/jgeot.18.P.047.

562 [30] Rollins, K.M., Evans, M.D., Diehl, N.B., and Daily III, W.D. 1998. Shear  
563 modulus and damping relationships for gravels. *Journal of Geotechnical and*  
564 *Geoenvironmental Engineering*, 124(5): 396-405.

565 [31] Seed, H.B., Wong, R.T., Idriss, I.M., and Tokimatsu, K. 1986. Moduli and  
566 damping factors for dynamic analyses of cohesionless soils. *Journal of*  
567 *Geotechnical Engineering*, 112(11): 1016-1032.

568 [32] Seif El Dine, B., Dupla, J.C., Frank, R., Canou, J., and Kazan, Y. 2010.  
569 Mechanical characterization of matrix coarse-grained soils with a large-sized  
570 triaxial device. *Canadian Geotechnical Journal*, 47: 425-438.

571 [33] Selig, E., and Waters, J. 1994. Track geotechnology and sub-structure  
572 management. Thomas Telford, London, U.K.

- 573 [34] Sevi, A., and Ge, L. 2012. Cyclic behaviors of railroad ballast within the parallel  
574 gradation scaling framework. *Journal of Materials in Civil Engineering*, 24(7):  
575 797-804.
- 576 [35] Suiker, A.S.J., Selig, E.T., and Frenkel, R. 2005. Static and cyclic triaxial testing  
577 of ballast and subballast. *Journal of Geotechnical and Geoenvironmental*  
578 *Engineering*, 131: 771-782.
- 579 [36] Tang, L., Yan, M.H., Ling, X.Z., and Tian, S. 2017. Dynamic behaviours of  
580 railway's base course materials subjected to long-term low-level cyclic loading:  
581 experimental study and empirical model. *Géotechnique*, 67(6): 537-545.
- 582 [37] Trinh, V.N. 2011. Comportement hydromécanique des matériaux constitutifs de  
583 plateformes ferroviaires anciennes. Ph.D. thesis, Ecole Nationale des Ponts et  
584 Chaussées, Université Paris-Est.
- 585 [38] Trinh, V.N., Tang, A.M., Cui, Y.J., Dupla, J.C., Canou, J., Calon, N., Lambert, L.,  
586 Robinet, A., and Schoen, O. 2012. Mechanical characterisation of the fouled  
587 ballast in ancient railway track sub-structure by large-scale triaxial tests. *Soils*  
588 *and Foundations*, 52(3): 511-523.
- 589 [39] Varadarajan, A., Sharma, K.G., Venkatachalam, K., and Gupta, A.K. 2003.  
590 Testing and modeling two rockfill materials. *Journal of Geotechnical and*  
591 *Geoenvironmental Engineering*, 129(3): 206-218.
- 592 [40] Wang, H.L., and Chen, R.P. 2019. Estimating static and dynamic stresses in  
593 geosynthetic-reinforced pile-supported track-bed under train moving loads.  
594 *Journal of Geotechnical and Geoenvironmental Engineering*, 145(7): 04019029.

- 595 [41] Wang, H.L., Chen, R.P., Cheng, W., Qi, S., and Cui, Y.J. 2019. Full-scale model  
596 study on variations of soil stress in geosynthetic-reinforced pile-supported  
597 track-bed with water level change and cyclic loading. *Canadian Geotechnical*  
598 *Journal*, 56(1): 60–68.
- 599 [42] Wang, H.L., Cui, Y.J., Lamas-Lopez, F., Dupla, J.C., Canou, J., Calon, N.,  
600 Saussine, G., Aïmedieu, P., and Chen, R.P. 2017. Effects of inclusion contents on  
601 resilient modulus and damping ratio of unsaturated track-bed materials. *Canadian*  
602 *Geotechnical Journal*, 54: 1672-1681.
- 603 [43] Wang, H.L., Cui, Y.J., Lamas-Lopez, F., Dupla, J.C., Canou, J., Calon, N.,  
604 Saussine, G., Aïmedieu, P., and Chen, R.P. 2018a. Permanent deformation of  
605 track-bed materials at various inclusion contents under large number of loading  
606 cycles. *Journal of Geotechnical and Geoenvironmental Engineering*, 144(8):  
607 04018044.
- 608 [44] Wang, H.L., Cui, Y.J., Lamas-Lopez, F., Calon, N., Saussine, G., Dupla, J.C.,  
609 Canou, J., Aïmedieu, P., and Chen, R.P. 2018b. Investigation on the mechanical  
610 behavior of track-bed materials at various contents of coarse grains. *Construction*  
611 *and Building Materials journal*, 164: 228-237.
- 612 [45] Werkmeister, S., Dawson, A.R., and Wellner, F. 2004. Pavement design model for  
613 unbound granular materials. *Journal of Transportation Engineering*, 130:  
614 665-674.
- 615 [46] Wichtmann, T., Rondon, H.A., Niemunis, A., Triantafyllidis, Th., and Lizcano, A.  
616 2010. Prediction of permanent deformations in pavements using a high-cycle

617 accumulation model. *Journal of Geotechnical and Geoenvironmental Engineering*,  
618 136: 728-740.

619 [47] Xiao, Y., Liu, H.L., Chen, Y.M., and Jiang, J.S. 2014. Bounding surface model  
620 for rockfill materials dependent on density and pressure under triaxial stress  
621 conditions. *Journal of Engineering Mechanics*, 140: 04014002.

622 [48] Yang, J., and Gu, X.Q. 2013. Shear stiffness of granular material at small strains:  
623 does it depend on grain size?. *Géotechnique*, 63(2): 165-179.

624 [49] Yang, L., Powrie, W., and Priest, J. 2009. Dynamic stress analysis of a ballasted  
625 railway track bed during train passage. *Journal of Geotechnical and*  
626 *Geoenvironmental Engineering*, 135(5): 680–689.

627 [50] Zeller, J., and Wullimann, R. 1957. The shear strength of the shell materials for  
628 the Göschenenalp Dam, Switzerland. *In Proceedings of the 4th International*  
629 *Conference on Soil Mechanics and Foundation Engineering*, London, pp.  
630 399-404.



## List of tables

Table 1. Mass proportions and grain size ranges of nine commercial soils

## List of Figures

Fig. 1. Grain size distributions of the ballast and the microballast (modified from Wang et al. 2018a)

Fig. 2. Grain size distributions of fines (modified from Wang et al. 2018a)

Fig. 3. Typical sine-shaped signals applied in the cyclic loadings

Fig. 4. Loading paths in two stages: (a) stage 1 for permanent strain investigation; (b) stage 2 for resilient modulus investigation

Fig. 5. Deviator stress  $q$  versus axial strain  $\varepsilon_1$  for the first 90,000 cycles of loading stage 1 (ballast specimen at  $f_v = 35\%$ )

Fig. 6. Permanent strain evolutions with number of cycles at different  $f_v$  values (ballast specimens)

Fig. 7. Illustration of the method to eliminate the loading history effect

Fig. 8. Measured and estimated permanent strain curves for ballast specimen at  $f_v = 0\%$

Fig. 9. Estimated permanent strain evolutions at the first 90,000 cycles for ballast specimen at  $f_v = 0\%$

Fig. 10. Variations of estimated end-stage permanent strains with  $f_v$  at different stress levels (ballast specimens)

Fig. 11. Hysteresis loops at first cycles of different stress levels for ballast specimen at

$f_v = 20\%$ :  $\Delta q = 10$  kPa ( $N = 1$ ),  $\Delta q = 30$  kPa ( $N = 101$ ),  $\Delta q = 50$  kPa ( $N = 201$ ),  $\Delta q = 100$  kPa ( $N = 701$ ) and  $\Delta q = 200$  kPa ( $N = 1401$ )

Fig. 12. Hysteresis loops during 100 cycles ( $N = 701$  to  $800$ ) under  $\Delta q = 100$  kPa for ballast specimen at  $f_v = 20\%$

Fig. 13. Determination of  $M_r$

Fig. 14. Evolution of  $M_r$  with number of cycles at different stress levels for ballast specimen at  $f_v = 20\%$

Fig. 15. Evolutions of  $M_r$  at end stage with  $f_v$  for ballast specimens at: (a)  $\Delta q = 10$  kPa; (b)  $\Delta q = 30$  kPa; (c)  $\Delta q = 50$  kPa; (d)  $\Delta q = 100$  kPa and  $200$  kPa

Fig. 16. Variations of estimated end-stage permanent strains with  $f_v$  for ballast and microballast specimens at: (a)  $\Delta q = 10$  kPa; (b)  $\Delta q = 15$  kPa; (c)  $\Delta q = 20$  kPa; (d)  $\Delta q = 25$  kPa and  $30$  kPa

Fig. 17. Schematic illustration of the distribution of fines soils in case of grain-grain contact structure

Fig. 18. Comparison of  $M_r$  value between ballast specimens and microballast specimens in case of fine-fine contact structure for: (a)  $f_v = 0\%$ ; (b)  $f_v = 5\%$ ; (c)  $f_v = 10\%$ ; (d)  $f_v = 20\%$

Fig. 19. Comparison of  $M_r$  value between ballast specimens and microballast specimens in case of grain-grain contact structure for (a)  $f_v = 35\%$  and (b)  $f_v = 45\%$

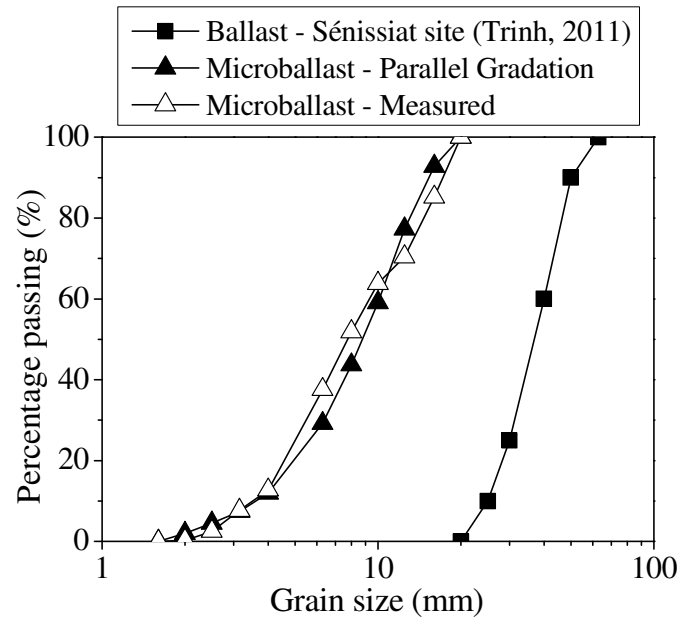


Fig. 1. Grain size distributions of the ballast and the microballast (modified from Wang et al. 2018a)

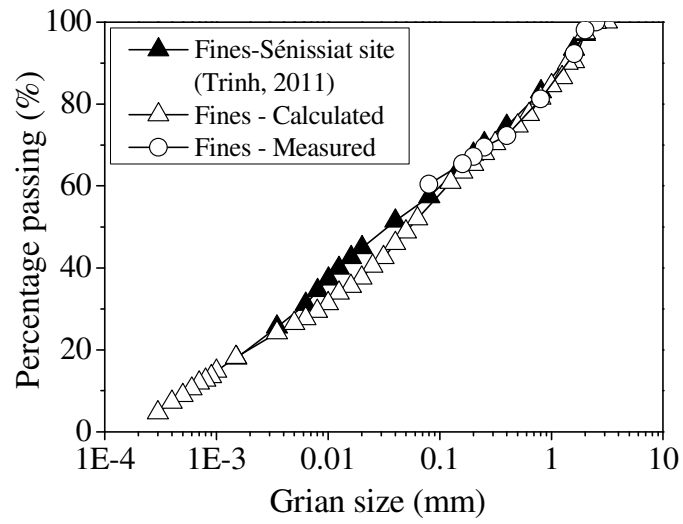


Fig. 2. Grain size distributions of fines (modified from Wang et al. 2018a)

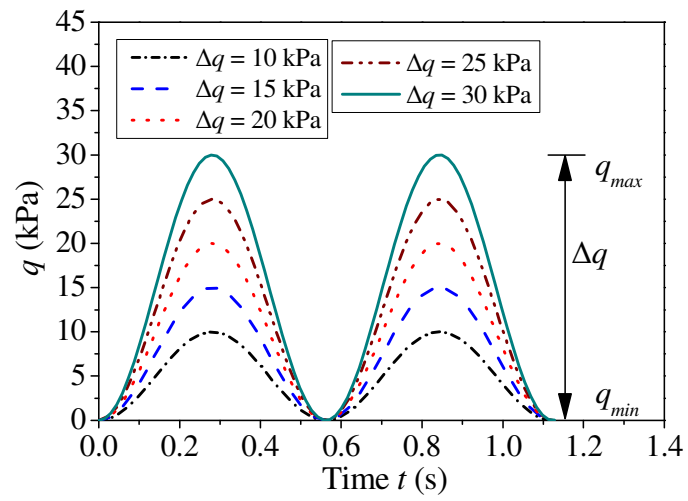


Fig. 3. Typical sine-shaped signals applied in the cyclic loadings

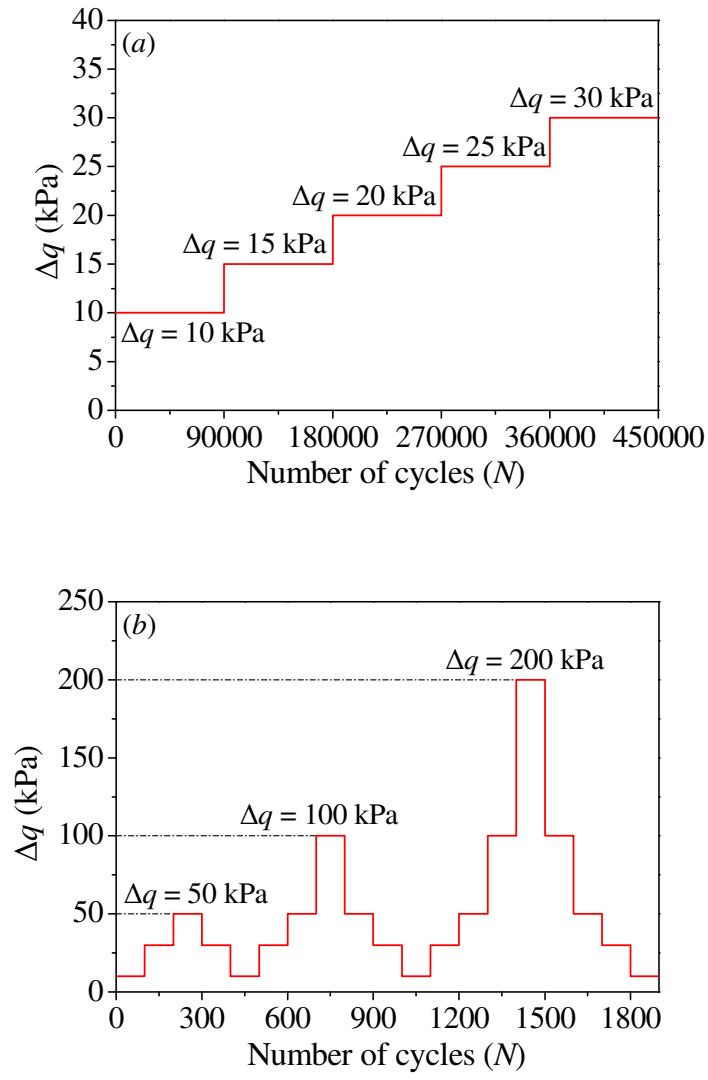


Fig. 4. Loading paths in two stages: (a) stage 1 for permanent strain investigation; (b) stage 2 for resilient modulus investigation

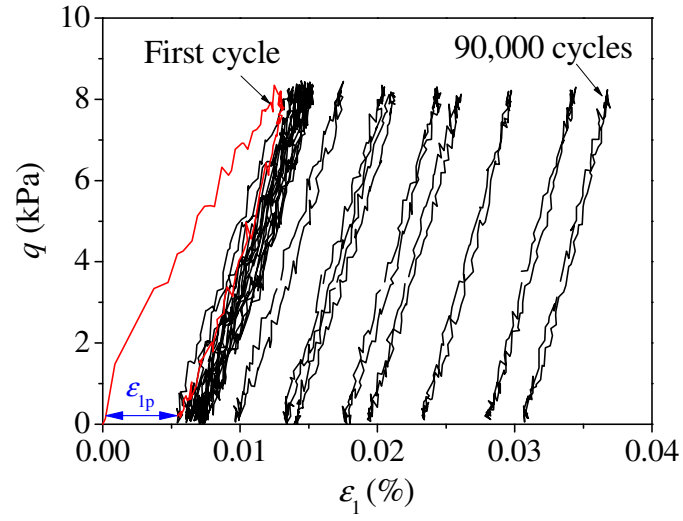


Fig. 5. Deviator stress  $q$  versus axial strain  $\varepsilon_1$  for the first 90,000 cycles of loading stage 1 (ballast specimen at  $f_v = 35\%$ )

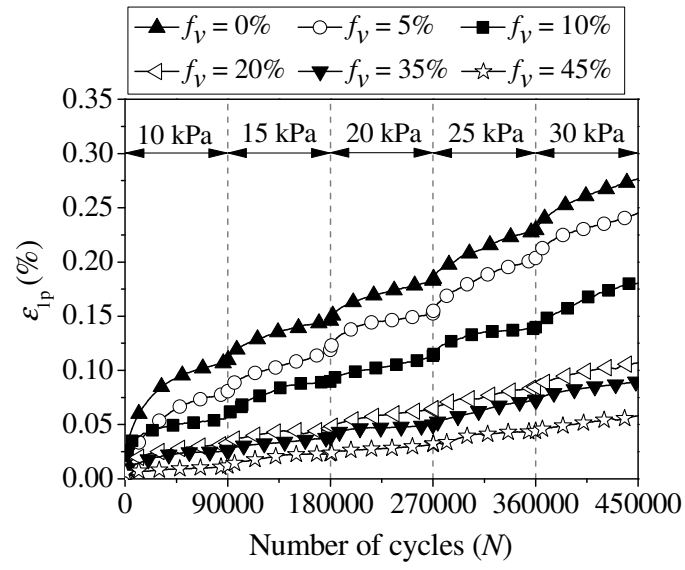


Fig. 6. Permanent strain evolutions with number of cycles at different  $f_v$  values

(ballast specimens)



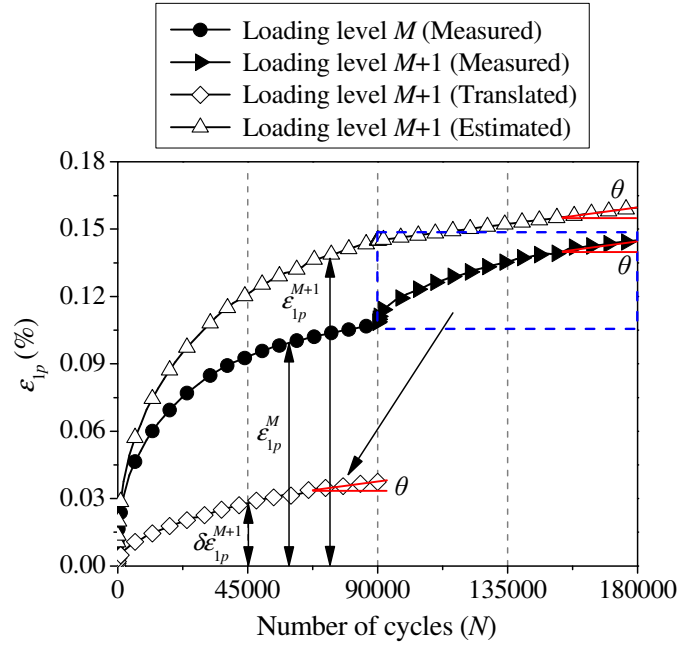


Fig. 7. Illustration of the method to eliminate the loading history effect

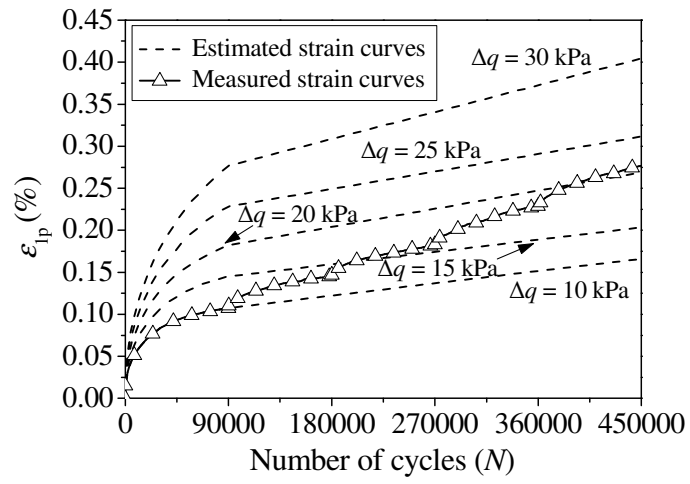


Fig. 8. Measured and estimated permanent strain curves for ballast specimen at  $f_v =$   
0%

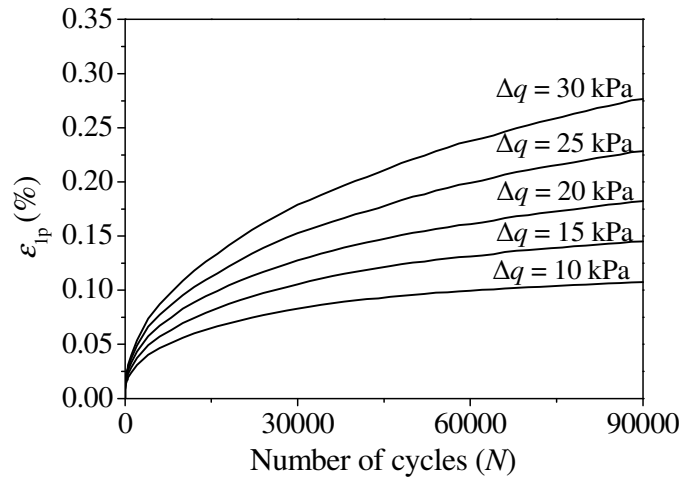


Fig. 9. Estimated permanent strain evolutions at the first 90,000 cycles for ballast specimen at  $f_v = 0\%$

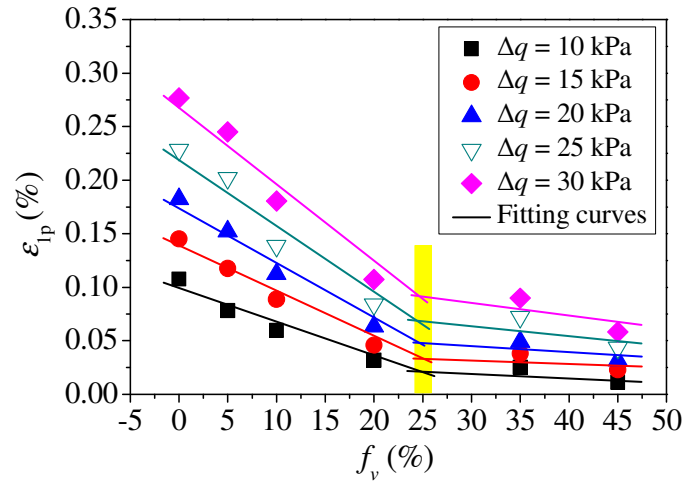


Fig. 10. Variations of estimated end-stage permanent strains with  $f_v$  at different stress levels (ballast specimens)

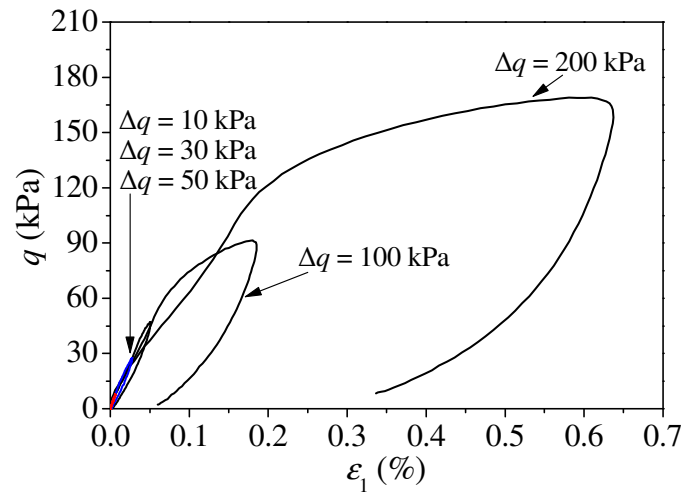


Fig. 11. Hysteresis loops at the first cycles of different stress levels for ballast specimen at  $f_v = 20\%$ :  $\Delta q = 10$  kPa ( $N = 1$ ),  $\Delta q = 30$  kPa ( $N = 101$ ),  $\Delta q = 50$  kPa ( $N = 201$ ),  $\Delta q = 100$  kPa ( $N = 701$ ) and  $\Delta q = 200$  kPa ( $N = 1401$ )

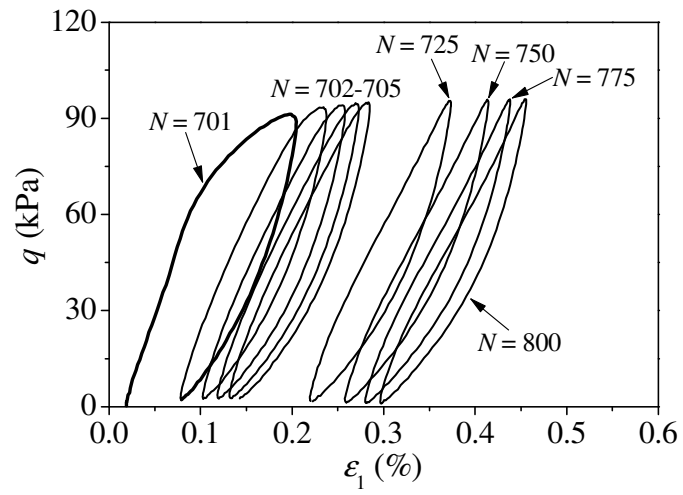


Fig. 12. Hysteresis loops during 100 cycles ( $N = 701$  to  $800$ ) under  $\Delta q = 100$  kPa for ballast specimen at  $f_v = 20\%$

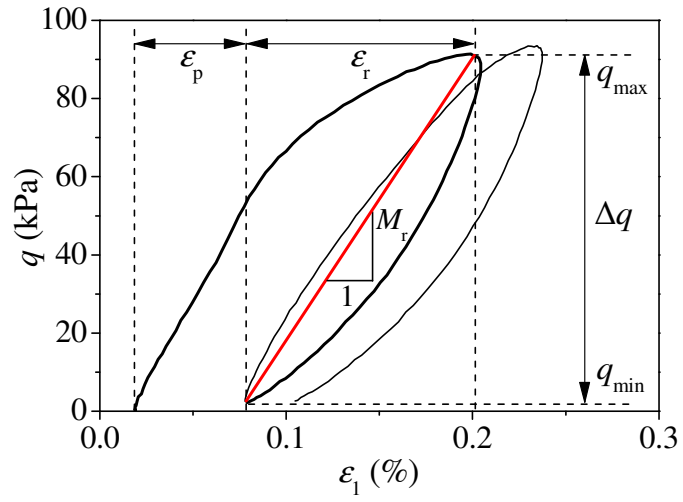


Fig. 13. Determination of  $M_r$

Note: The two hysteresis loops shown are the testing results of ballast specimen at  $f_v = 20\%$  under  $\Delta q = 100$  kPa at cycle numbers of  $N = 701$  and  $702$ .

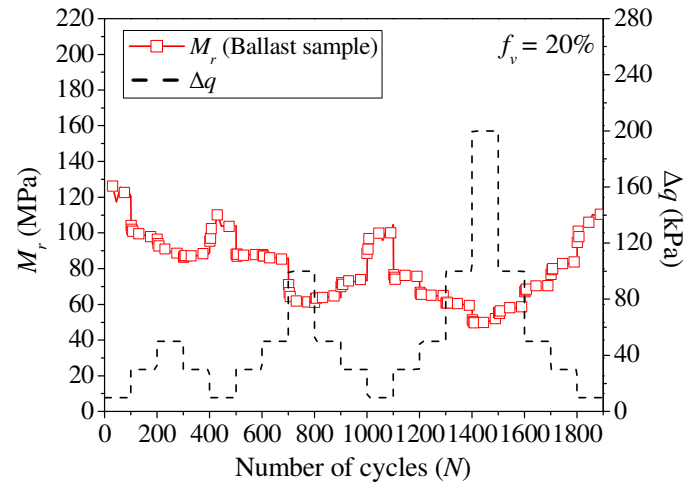


Fig. 14. Evolution of  $M_r$  with number of cycles at different stress levels for ballast specimen at  $f_v = 20\%$



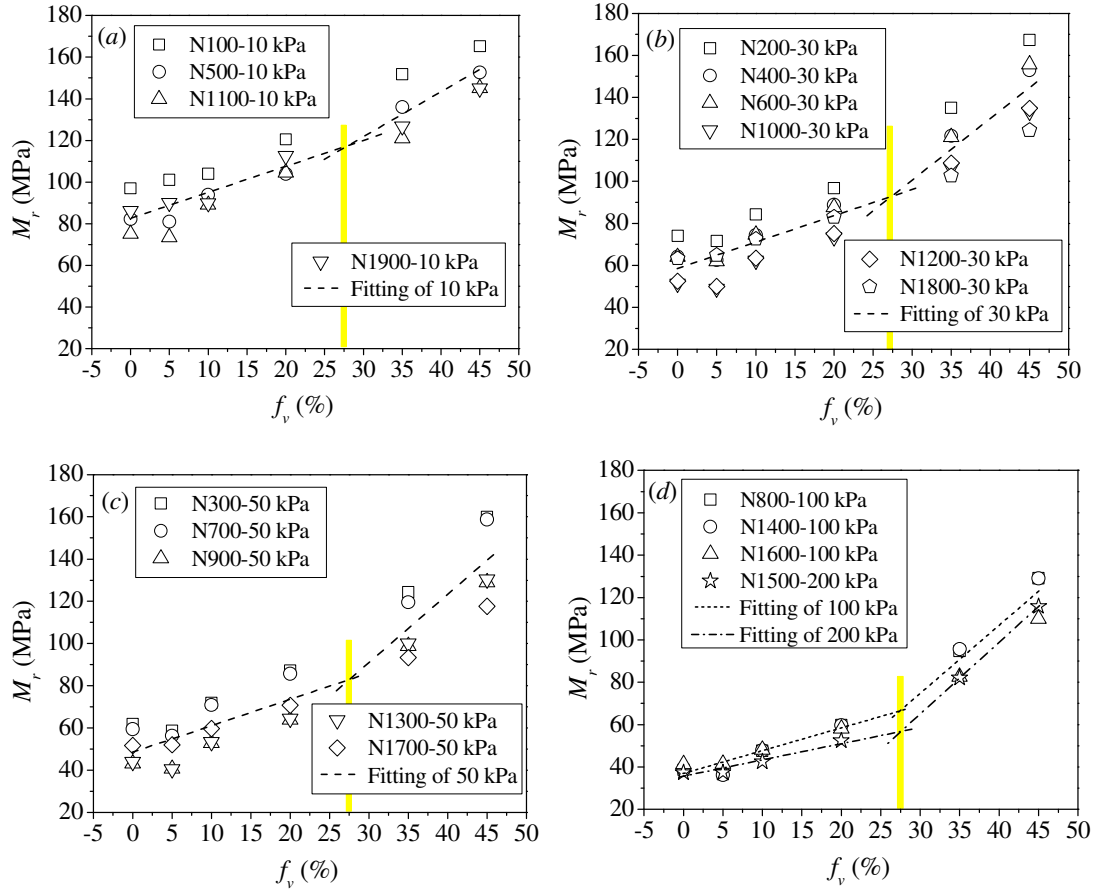


Fig. 15. Evolutions of  $M_r$  at end stage with  $f_v$  for ballast specimens at: (a)  $\Delta q = 10$  kPa; (b)  $\Delta q = 30$  kPa; (c)  $\Delta q = 50$  kPa; (d)  $\Delta q = 100$  kPa and 200 kPa

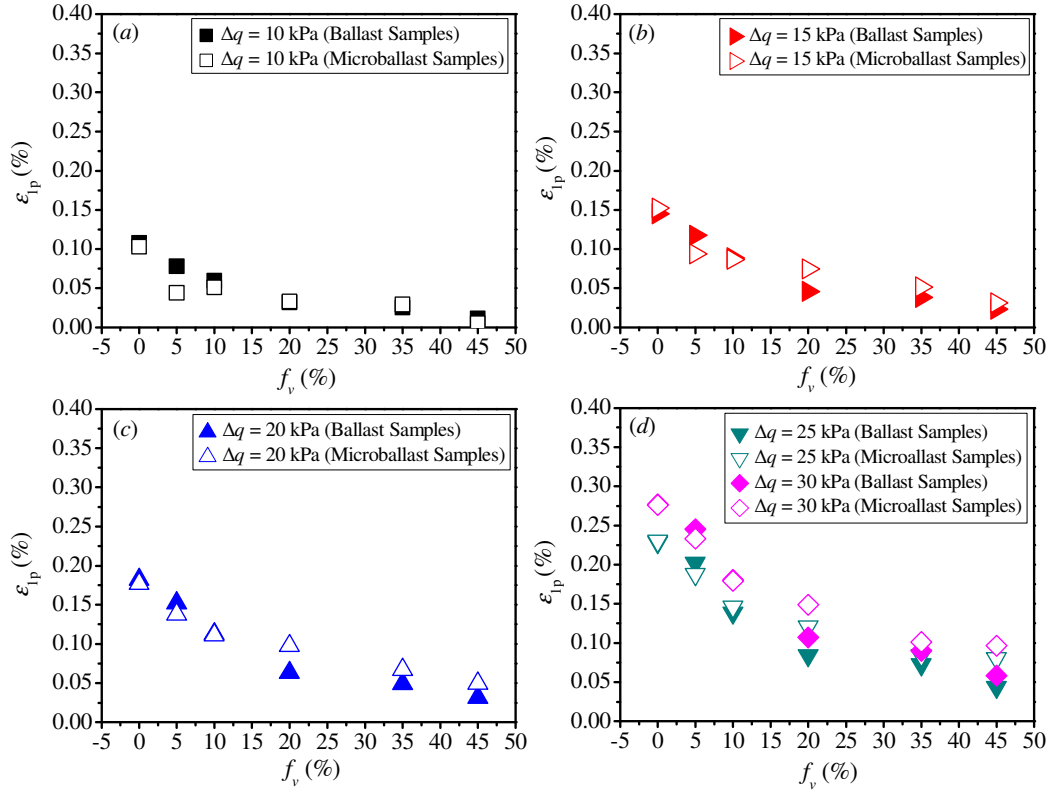


Fig. 16. Variations of estimated end-stage permanent strains with  $f_v$  for ballast and microballast specimens at: (a)  $\Delta q = 10$  kPa; (b)  $\Delta q = 15$  kPa; (c)  $\Delta q = 20$  kPa; (d)  $\Delta q = 25$  kPa and  $30$  kPa

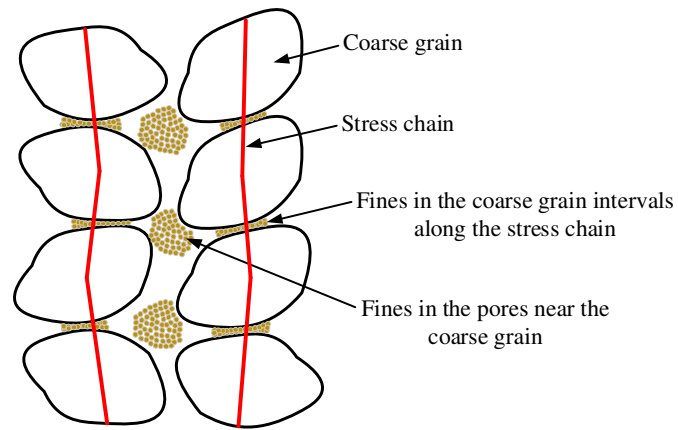


Fig. 17. Schematic illustration of the distribution of fines soils in case of grain-grain  
contact structure

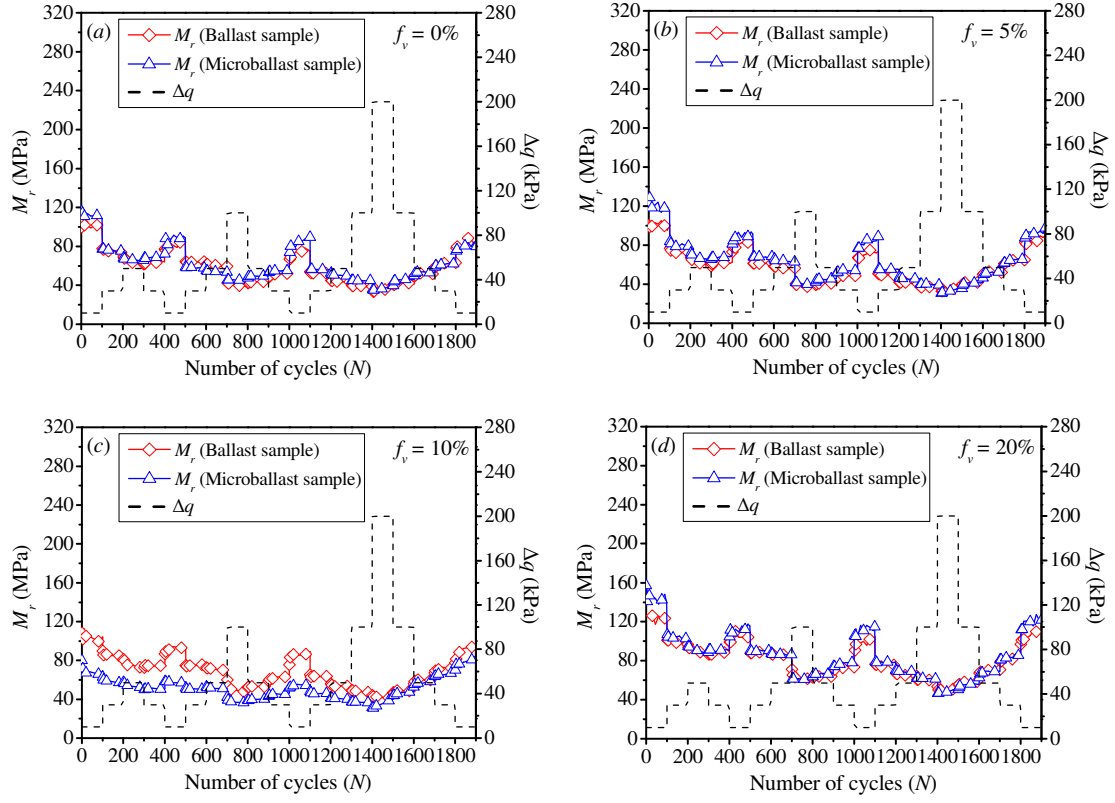


Fig. 18. Comparison of  $M_r$  value between ballast specimens and microballast specimens in case of fine-fine contact structure for: (a)  $f_v = 0\%$ ; (b)  $f_v = 5\%$ ; (c)  $f_v = 10\%$ ; (d)  $f_v = 20\%$

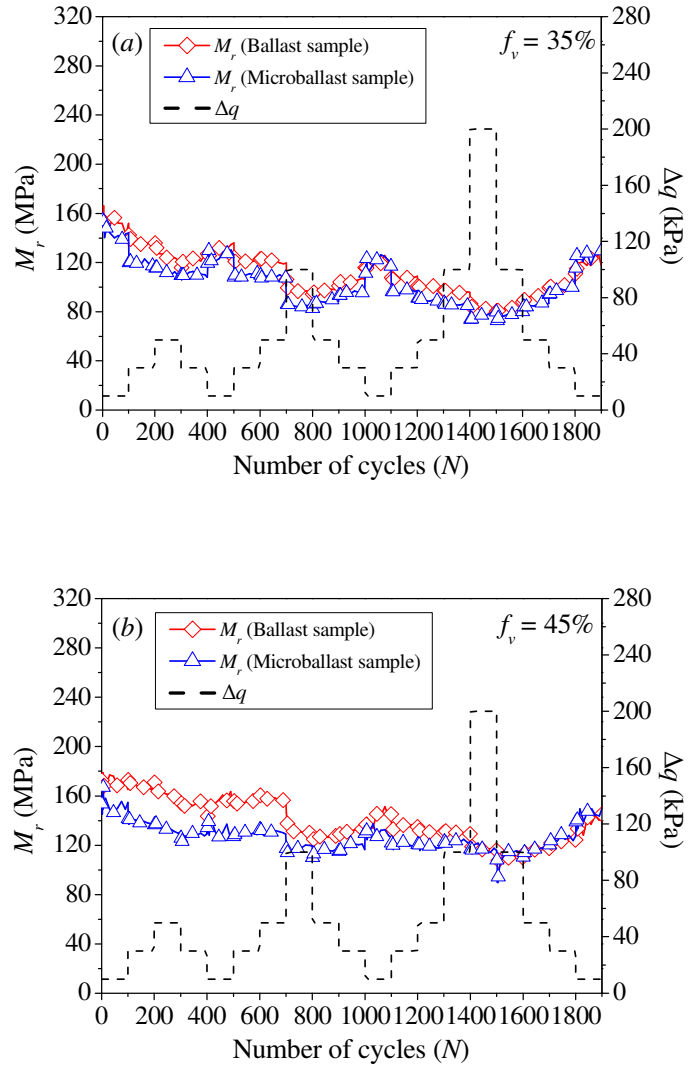


Fig. 19. Comparison of  $M_r$  value between ballast specimens and microballast specimens in case of grain-grain contact structure for (a)  $f_v = 35\%$  and (b)  $f_v = 45\%$

Table 1. Mass proportions and grain size ranges of nine commercial soils

---

0.001 - 0.01 (20% of the particles)

0.0003 - 0.01 (80% of the particles)

0.0009 - 0.25

0.0009 - 0.50

0.063 - 0.50

0.16 - 0.63

0.25 - 1

0.32 - 2

0.32 - 3.20

---